Research Article | Vol. 28, No. 24 / 23 November 2020 / Optics Express 35784
Optics EXPRESS

Design of efficient radiative emission and daytime cooling structures with Si_3N_4 and SiO_2 nanoparticle laminate films

PARKER R. WRAY,[1] MAGEL P. SU,[2] AND HARRY A. ATWATER[2,*]

[1]Department of Electrical Engineering, California Institute of Technology, Pasadena, CA 91125, USA
[2]Department of Applied Physics and Materials Science, California Institute of Technology, Pasadena, CA 91125, USA
*haa@caltech.edu

Abstract: Research on radiative cooling has attracted recent widespread interest owing to the potential for low-cost passive structures to enable large-scale thermal energy management. Using a generalized effective medium theory, we theoretically show that two-layer films comprised of SiO_2 and Si_3N_4 nanoparticle layers on an Ag back reflector exhibit superior radiative cooling compared to single-layer or two-layer dense solid films, and can outperform other reported designs. The performance enhancement is a result of the ability to tune the nanoparticle fill fraction, which improves the spectral match between emissivity of this structure and the atmospheric transmission window. We also propose a standardized method for comparing the performance of radiative cooling structures reported by the research community.

1. Introduction

Approximately forty percent of the world population lives in consistently hot regions, many of which have homes lacking air conditioning [1–3]. Rising standards of living and growing demand for improved public health and comfortable living conditions is projected to lead to a 450% increase in air conditioning from 2010 to 2050 worldwide, representing one of the largest contributors to worldwide energy consumption [4–6]. Furthermore, current air conditioning systems account for almost 700 million metric tons of CO_2-equivalent emissions per year [2]. Seventy-four percent of these emissions are from electricity generation and approximately nineteen percent from refrigerant based hydrochlorofluorocarbons (HCFCs) which have a disproportionately large global warming impact relative to their mass [2]. These predictions highlight the importance of developing improved sustainable and environmentally friendly cooling technologies. Furthermore, a low cost and easily implemented passive cooling technology can promote early adoption in developing countries, reduce overall energy use, and lower greenhouse gas emissions.

Cooling by radiative heat transfer from a terrestrial ambient to the cold ambient of space is a passive, sustainable solid-state technique to provide cooling without the need for external power or additional operating costs. Photonic structures which are both highly reflective in the solar spectrum (below 2.5 μm) and highly emissive in the infrared atmospheric transmission window (8–14 μm) can suppress solar heating and remove heat through infrared (IR) radiation to cool throughout the diurnal cycle. Radiative cooling structures are particularly applicable in regions with low humidity, where the atmosphere is most transparent, such as Mexico, northern and southern Africa, the Middle East, Australia, India, parts of North and South America, and areas of northern Asia [2,7]. The primary requirement of a radiative cooler is to provide enough cooling power at a specified temperature to more than offset its own parasitic heating, thus providing net cooling, and is constrained by the limited bandwidth of the infrared atmospheric transmission window and stringent reflectivity requirements in the solar spectrum. Recent designs

#408845 https://doi.org/10.1364/OE.408845
Journal © 2020 Received 31 Aug 2020; revised 9 Oct 2020; accepted 27 Oct 2020; published 10 Nov 2020

Optics EXPRESS

for daytime radiative cooling structures to improve cooling performance include structures with glass nanoparticles embedded into a polymer film, layered thin films on back reflectors, and complex lithographically patterned structures such as many-layered nanoarrays [8–19]. Other passive cooling techniques – such as earth to air heat exchangers, evaporative coolers, and nocturnal convective coolers – focus on removing heat through a heat sink (ground, water, or air respectively), but suffer from high initial costs, continual operating costs, and/or external power requirements [20,21].

Films composed of Rayleigh scattering nanoparticles can provide simple photonic designs for improving daytime cooling performance and are amenable to scalable manufacturing [22,23]. By tuning the nanoparticle fill fraction, air-material composites of this type can provide broadband impedance matching to free space and the ability to spectrally tune absorption resonances by changing the local (Lorentz) field [24–26]. Conversely, layered structures synthesized by thin film deposition can enable improved impedance matching to free space and resonance shifts through either graded index stacks, periodic layered structures, or intricate patterning [27–30]. For graded index and periodic structures, impedance matching is limited by the minimum practically achievable refractive index in the low index layers and the number of layers in the stack [27]. Furthermore, graded index and periodic layered structures are constrained by the limited portfolio of materials that can be used to achieve the stringent broadband reflection and emission requirements of a daytime radiative cooler [31]. Use of patterned subwavelength-scale resonant or wavelength-scale diffractive photonic structures represents another approach to tune photonic properties but is limited by fabrication complexity for large-area low-cost structures [31]. In this paper, we theoretically show that nanoparticle films can circumvent the impedance matching and materials limits which constrain layered structures. Two-layer nanoparticle films can achieve radiative cooling performance comparable to or greater than others reported to date, based solely on tuning nanoparticle fill fraction and film thickness.

Using a generalized effective medium theory, we show that simple two-layer nanoparticle films composed of separate layers of SiO_2 and Si_3N_4 particles on a silver back reflector can outperform all dense solid laminate thin films and provide a cooling performance superior to those reported previously [8–12]. Using consistent solar, atmospheric, convective/conductive, and ambient temperature conditions across comparisons, we find that the radiative cooling performance of two-layer nanoparticle film designs exceeds many reports of radiative cooling designs in literature by up to 20 W/m^2 and 25 W/m^2 at operating temperatures of 290 K and 280 K respectively. Furthermore, optimized two-layer nanoparticle film designs have higher cooling power than optimized dense solid laminate thin films, regardless of which structure or composition is chosen. These results support the idea that random nanoparticle laminate films could provide a feasible alternative to dense solid thin film or patterned designs, provided scalable synthesis techniques can be identified. In this regard, plasma synthesis or ball milling could be considered as possible scalable deposition methods [22,32].

2. Defining an optimal radiative cooler

There are three important factors to consider when designing a daytime radiative cooling structure, which can be inferred from Eq. (S1)–(S6)in the Supplement. First, the criterion for defining an optimal radiative cooling structure should be to maximize the structure's net cooling power at a desired target operating temperature, called the "optimization temperature". Second, the performance of a radiative cooling structure is fundamentally limited by the atmospheric emission spectrum. As such, the atmospheric emission spectrum of the target operating environment needs to be carefully considered. Third, to achieve cooling below ambient temperature, solar absorption and other forms of parasitic heating must be kept below a critical threshold.

Optics EXPRESS

We can define the theoretical spectral emission of an optimal radiative cooling structure as

$$e_r(\lambda, T_r, T_a, \theta, \alpha) = \begin{cases} 1, & I_B(\lambda,\ T_r) > I_B(\lambda, T_a) e_a(\lambda, \theta, \alpha) \\ 0, & else \end{cases} \tag{1}$$

where e_r is the emissivity of the structure, e_a is the emissivity of the atmosphere, λ is the free space wavelength, T_r is the structure's temperature, T_a is the ambient temperature, θ is the angle of emission, and α is a variable encapsulating the conditions relating to the composition of the atmosphere [33]. I_B is defined as the blackbody spectral radiance

$$I_B = \frac{2hc^2}{\lambda^5} \frac{1}{e^{\frac{hc}{\lambda k_B T}} - 1} \tag{2}$$

where h is Plank's constant, k_B is the Boltzmann constant, and c is the speed of light. Equation (1) shows that the theoretical optimal cooling performance is a function of the temperature of the radiative cooling structure, ambient temperature, emission angle, and atmospheric composition.

In regard to choosing the appropriate atmospheric emission spectrum, Fig. 1(a) shows the atmospheric transmission windows from the Gemini Observatory (low humidity level) and from the 1976 United States Standard (average humidity level) [34]. The spectra at the Gemini Observatory represents near ideal conditions where a radiative cooler with high emissivity in both the first (8–14 μm) and second (16–24 μm) atmospheric transmission windows could achieve the highest possible cooling power. However, it is shown in Fig. 1(a) that while two atmospheric transmission windows exist at very low humidity levels, the prevalence of water molecules in the atmosphere greatly diminishes the contribution of the second atmospheric transmission window towards radiative cooling for most areas of the world [35]. Consequently, practical radiative coolers in terrestrial applications should optimize emission only in the first atmospheric transmission window and over all angles. The 1976 United States Standard atmospheric emission spectrum was modeled using LOWTRAN7, an open-source software comparable to MODTRAN [36–38]. Figure 1(b) shows the 1976 United States Standard atmospheric emission spectra at 300 K with blackbodies of 300 K, 280 K, 260 K, and 240 K overlaid in the background [35]. From Fig. 1(b), we see that the optimal emission window as described in Eq. (1) for achieving maximum cooling power is denoted by the area of each blackbody that is not overlapped by the atmospheric emittance. This demonstrates the dependence of the optimal spectral emission window on the operating temperature. Figure 1(c) illustrates the radiative cooling power (P_r) to operating temperature relationship for ideal radiative coolers as defined by Eq. (1). Each solid curve is the radiative cooling power based on spectral emission windows optimized for 300 K, 280 K, 260 K, and 240 K blackbodies minus the atmospheric heating (P_a), at an ambient temperature of 300 K. From the solid curves in Fig. 1(c), we see that each optimal spectral emission window achieves a superior cooling power compared to its peers when operating at or near its optimization temperature. The dashed horizontal lines show the net-zero power curves ($P_{net} = 0$) for different percentages of solar absorption (P_{sun}). From these dashed lines, we find that radiative cooling while operating below the ambient temperature of 300 K is effectively impossible if parasitic solar absorption is higher than 10%. The dashed sloped lines show $P_{net} = 0$ when considering different non-radiative heat transfer coefficients (q), which account for convective and conductive heat transfer (P_{other}). The overall $P_{net} = 0$ line is determined by a linear combination of the solar absorption and non-radiative heat transfer effects.

Optics EXPRESS

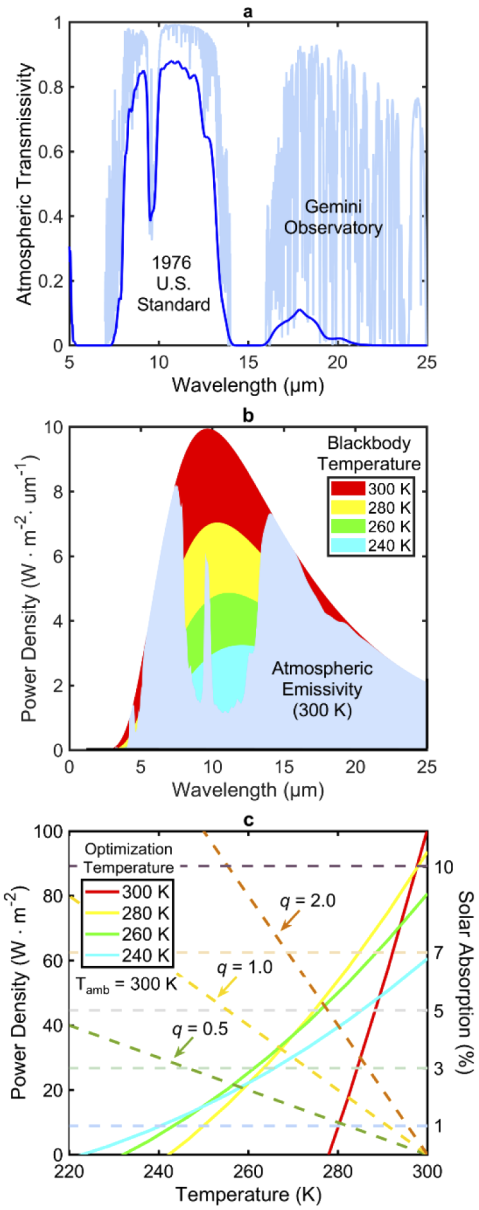

Fig. 1. (a) Atmospheric transmission spectra at low humidity taken from the Gemini Observatory and at average humidity taken from the 1976 U.S. Standard; (b) blackbody spectra at various temperatures (300 K, 280 K, 260 K, and 240 K) overlaid on the atmospheric emission spectrum from 1976 U.S. Standard at 300 K; (c) radiative cooling power density versus operating temperature relationship for the four theoretically optimal radiative cooling spectral emission windows defined from (b), each is optimized to provide superior cooling power at a specific optimization temperature under ambient conditions (300 K). The solid lines show radiative cooling power (P_r) minus atmospheric heating (P_a) versus operating temperature for each of the optimal radiative coolers. Solar absorption percent is given by the horizontal dashed lines. Losses from conduction and convection for various non-radiative heat transfer coefficients (q), are marked with sloping dashed lines. The total net zero cooling power line is represented by a linear combination of the solar absorption line and non-radiative heat transfer coefficient line.

Optics EXPRESS

3. Radiative cooling in SiO_2 and Si_3N_4 nanoparticle laminate films

Using a generalized effective medium theory, we design different radiative cooling structures comprised of separate layers of SiO_2 and Si_3N_4 nanoparticle films with air as the matrix medium. We find that two-layer nanoparticle films always outperform dense solid laminate thin films and are sufficient to achieve cooling performances greater than or similar to previously reported structures [8–12]. In our designs, SiO_2 and Si_3N_4 were chosen as the emissive materials because of their strongly peaked absorption within the atmospheric transmission window. Specifically, in-phase and out-of-phase stretching of the Si–O bond is responsible for the strong absorption peak in SiO_2 from 8–10 μm, and Si–N bond stretching is responsible for the broad absorption peak in Si_3N_4 from 9–15 μm [39–42]. In both cases the absorption coefficient for wavelengths between 0.25–5 μm can be made negligibly small. The generalized effective medium permittivity, considering a single type of inclusion, is given by:

$$\frac{\varepsilon_{eff}-\varepsilon_e}{2\varepsilon_e+\varepsilon_{eff}+\nu(\varepsilon_{eff}-\varepsilon_e)} = f\frac{\varepsilon_i-\varepsilon_e}{2\varepsilon_e+\varepsilon_i+\nu(\varepsilon_{eff}-\varepsilon_e)} \tag{3}$$

where ε_e is the host permittivity (free space in this case), ε_i is the inclusion permittivity (SiO_2 or Si_3N_4), f is the inclusion fill fraction, ε_{eff} is the resulting effective permittivity, and ν is a continuous variable which encapsulates how the inclusion responds to the internal field. Using this framework, the Maxwell Garnett (MG) formula is recovered at $\nu = 0$, Bruggeman at $\nu = 2$, and Coherent Potential (CP) at $\nu = 3$ [43]. Therefore, this generalized formula spans a set of effective medium theories and values of ν between the common theories can be viewed as a hybrid response in the internal field. For each structure designed, we span ν to compare the structure's cooling performance under each effective medium formula and hybrid parameters. As a representative example Fig. 2(a)–2(e) show the real (n) and complex (k) refractive index for bulk SiO_2 and Si_3N_4 as well as the effective n_{eff} and k_{eff} for laminate nanoparticle films of SiO_2 or Si_3N_4 as a function of fill fraction under the Bruggeman formula [43,–45]. Figure 2(a)–2(b), 2(d)–2(e) show that by tuning the nanoparticle fill fraction, we can reduce impedance mismatch between the nanoparticle film and free space. We can also spectrally shift the location of maximum k_{eff} of the material composite as a result of coupling between phonons and the internal field [24–26]. Figure 2(c) and Fig. 2(f) emphasize the effect of spectral shifting by normalizing the amplitude of k_{eff} for SiO_2 and Si_3N_4 laminate nanoparticle films within the atmospheric transmission window, respectively. Both increased impedance matching and spectral absorption resonance shifting are found to be consistent features no matter the choice of ν. We note that SiO_2 and Si_3N_4 nanoparticles with diameters of 50 nm or less satisfy the condition of Rayleigh scattering throughout the visible and IR wavelength regime [46]. Under this condition, the effective medium theory given by Eq. (3) is valid [24–26,47–51]. Synthesis of nanoparticle films composed of nanoparticles of this size and smaller, and with sufficiently narrow size distributions and high uniformity, can be done via both dusty plasma synthesis and ball milling [32,52–55]. We set a 60% fill fraction as a realistic upper limit due to the theoretical limit of random sphere packing (62–64%) [56,57].

We also study the limits an effective permittivity for a random particle film can be, which is determined from the Hashin-Shtrikman (HK) bounds:

$$\varepsilon_{MG} \leq \varepsilon_{eff} \leq \varepsilon_{MG-Comp} \tag{4}$$

where the lower limit is given by the MG formula and the upper limit by the MG formula of the complementary structure in which the host and medium materials are transposed. Thus, Eq. (4) gives an estimate on the permittivity extrema we may encounter for nanoparticle laminate films, and Eq. (3) provides the framework to model the behavior of these films under an entire class of effective medium theories within the HK bounds. From this framework, we can compare two-layer SiO_2 and Si_3N_4 laminate nanoparticle films to dense solid thin film equivalents.

Optics EXPRESS

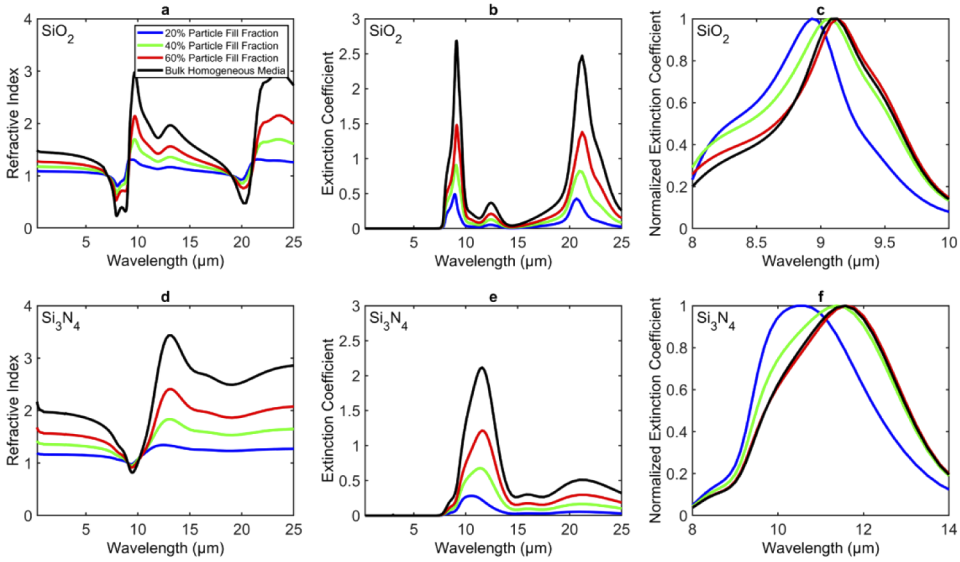

Fig. 2. (a), (b) n_{eff} and k_{eff} for SiO_2 at various fill fractions with air as the matrix medium; (c) normalized k_{eff} for SiO_2 within atmospheric transmission window demonstrating spectral shifting as a function of fill fraction; (d), (e) n_{eff} and k_{eff} for Si_3N_4 at various fill fractions with air as the matrix medium; (f) normalized k_{eff} for Si_3N_4 within the atmospheric transmission window demonstrating spectral shifting as a function of fill fraction.

Using transfer matrix calculations, we determine each structure's wavelength, angle, and polarization-resolved absorption/emission profile, then calculate its net radiative cooling power (P_{net}) as a function of operating temperature [58,59]. Optimal designs for each temperature regime were found by systematically varying each laminate nanoparticle layer thickness, fill fraction, material orientation (alternating the material of the top and bottom layers), and film type (laminate nanoparticle film or dense solid thin film) for all permutations of two-layer structures of SiO_2 and Si_3N_4 on an Ag back reflector. As such, a total of 32 two-layer radiative cooling structures were optimized. At each of four optimization temperature (300 K, 290 K, 280 K, 270 K), we optimized eight unique two-layer structures on a silver back reflector based on material order (SiO_2 on Si_3N_4 or Si_3N_4 on SiO_2) and film type (two thin film layers, thin film on laminate nanoparticle film, laminate nanoparticle film on thin film, and two laminate nanoparticle films). Figure 3(a) shows an example schematic of a radiative cooling structure comprised of two layers of laminate nanoparticle films on a silver back reflector. The specific design parameters (layer thickness, fill fraction) and radiative cooling powers for all 32 optimized radiative cooling structures can be found in Tables (S1)–(S18) in the Supplement.

Figure 3(b) shows the radiative cooling power of each of the 32 optimized two-layer radiative cooling structures under the Bruggeman mixing rule ($\nu = 2$). Each structure is shown at the operating temperature where their spectra has been optimized to give the most cooling power (optimization temperature). We assume an ambient of 300 K and account for solar absorption. No conduction or convection losses ($q = 0$) are shown as they would be common to each structure and are not an aspect of the photonic design. From Fig. 3(b), we see that optimized two-layer laminate nanoparticle films on a silver back reflector outperform optimized two-layer dense solid thin films at all optimization temperatures. The best performing two-layer laminate nanoparticle film structures show a 40% to 120% increase in radiative cooling power compared to the best performing two-layer dense solid thin film structures. The laminate nanoparticle films also demonstrate cooling at 270 K, which is unachievable in a dense solid thin film structure.

Optics EXPRESS

Figure 3(c) shows the radiative cooling power of each of 32 optimized two-layer radiative cooling structures under the Maxwell Garnett mixing rule. From Fig. 3(c), we see that optimized two-layer laminate nanoparticle films on silver back reflector are still predicted to outperform optimized two-layer dense solid thin films at all target temperatures, with increases of 30% and 109% in radiative cooling power when using the Maxwell Garnett mixing rule. Using the design parameters for the best performing two-layer laminate nanoparticle film and its two-layer thin film analog at each optimization temperature, we show in Fig. 3(d) the radiative cooling power of the laminate nanoparticle films when calculated using different effective medium formulas ($v = 0, 1, 2, 3$). Results from the HK bounds and the optimal thin film design are also plotted. From Fig. 3(d) we see that laminate nanoparticle films have higher predicted radiative cooling powers than two-layer thin film structures of the same material at all operating temperatures regardless of the effective medium theory used. In all cases, the AM1.5 solar spectrum was used, and the atmospheric transmittance data was taken from the 1976 U.S. Standard using

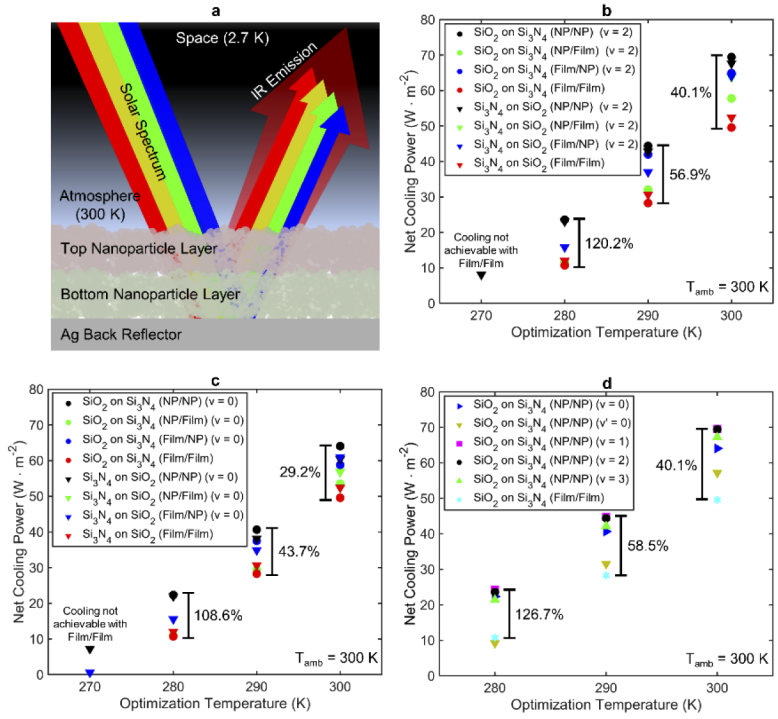

Fig. 3. (a) Schematic of radiative cooler comprised of two layers of laminate nanoparticle films on a silver back reflector; (b) net radiative cooling power of all 32 optimal two-layer nanoparticle film, thin film, or nanoparticle and thin film composite structures of SiO_2 and Si_3N_4 operating at their optimization temperature calculated using the Bruggeman effective medium formula ($v = 2$); (c) net radiative cooling power of all 32 optimal two-layer nanoparticle film, thin film, or nanoparticle and thin film composite structures of SiO_2 and Si_3N_4 operating at their optimization temperature calculated using the Maxwell Garnett effective medium formula ($v = 0$); (d) net radiative cooling power versus optimization temperature for the optimal two-layer nanoparticle films calculated using different effective medium theories. The nanoparticle film structure performance is compared to the two-layer thin-film analog to demonstrate that superior radiative cooling power is predicted regardless of which effective medium formula is used. All figures assume an ambient temperature of 300 K and no conduction or convection losses ($q = 0$).

Optics EXPRESS

LOWTRAN7 [34,36,60], integrated over angle and wavelength for both polarizations, and the ambient temperature was 300 K. Non-radiative heat losses were not considered since these losses would be common since film thicknesses are negligible for heat capacitance, the losses can be and often are controlled by the design of an external box, and are not inherent to the photonic aspects of the design. This does not detract from the comparison. The angular, spectral, and polarization-resolved emissivity profiles for all two-layer laminate nanoparticle film structures as calculated by both Bruggeman and Maxwell Garnett effective medium formulas can be found in Fig. S1 –S8 in the Supplement.

Figure 4 compares the cooling performance of the optimal two-layer laminate nanoparticle films from Fig. 3(a) under the mixing rule to structures that have been previously reported [8–11,18]. In order to provide a direct comparison, absorptivity/emissivity curves from previous reports are digitized and the radiative cooling performance is compared using the same AM1.5 solar spectrum and atmospheric absorption spectrum (the 1976 U.S. Standard) [34]. Furthermore, all calculations use an ambient of 300 K, and no non-radiative heat losses were considered. Therefore, the results should be interpreted as the relative average performance based on United States standards. Since multiple papers only report emissivity curves at normal incidence, all calculations assume the structure emits as a Lambertian surface [8–11,18]. We then perform the angular integration found in Eq. (S2)–(S4) under this assumption, allowing us to account for the angular dependence of the 1976 U.S. Standard atmospheric spectra. While the lack of angular information will alter the achievable cooling power, applying the approximation of Lambertian emittance allows for a consistent comparison between curves. Non-radiative heat losses were not considered since these losses are or can be controlled by the design of an external box and are not inherent to the photonic aspects of the design. Solar absorption is considered since it is part of the photonic design for daytime cooling. The results suggest that laminate nanoparticle film structures can provide cooling performance superior to other reported radiative cooling structures at temperatures below a 300 K ambient, many of which are achieved only through complex photonic designs.

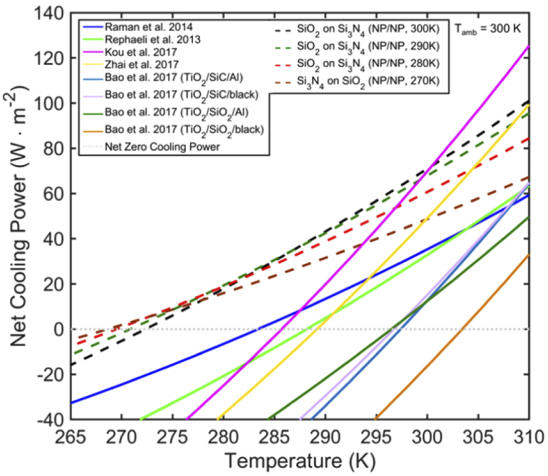

Fig. 4. Comparison between various radiative structure performances from literature (solid) and proposed two-layer radiative cooling structures composed of SiO_2 and Si_3N_4 laminate nanoparticle films on silver back reflector (dashed). Each dashed curve represents a unique two-layer radiative cooler optimized for a different operating temperature. Literature curves are obtained through digitization of published emissivity data at normal incidence and it is assumed the emissivity is angle independent. This figure serves purely as a guide for visualizing the relative benefit of nanoparticle films in radiative cooling.

Optics EXPRESS

4. Conclusion

We have demonstrated that SiO_2 and Si_3N_4 two-layer nanoparticle laminate films can give rise to radiative cooling powers that are higher than the best dense solid thin film laminate designs using the same materials. This result is robust with respect to the effective medium theory employed for optimization. Furthermore, we show that simple two-layer nanoparticle structures are sufficient to achieve cooling performances exceeding that of previously reported designs. Cooling performance improvements ranging from 20 W/m^2 to 25 W/m^2 over previously reported designs are possible with two-layer laminate nanoparticle films at operating temperatures of 290 K and 280 K respectively, and two-layer laminate nanoparticle films remain competitive with previously reported designs at 300 K. This work suggests that nanoparticle laminate films are a promising component for future simple, scalable, and effective daytime radiative cooling structures.

Funding

Army Research Office (W911NF-18-1-0240).

Acknowledgments

Atmospheric transmission data in Fig. 1(a) was based on observations obtained at the Gemini Observatory acquired through the Gemini Science Archive, which is operated by the Association of Universities for Research in Astronomy, Inc., under a cooperative agreement with the NSF on behalf of the Gemini partnership: the National Science Foundation (United States), National Research Council (Canada), CONICYT (Chile), Ministerio de Ciencia, Tecnología e Innovación Produc-tiva (Argentina), Ministério da Ciência, Tecnologia e Inovação (Brazil), and Korea Astronomy and Space Science Institute (Republic of Korea).

Disclosures

The authors declare no conflicts of interest.

See Supplement 1 for supporting content.

References

1. International Energy Agency, "The future of cooling," IEA, Paris (2018).
2. W. Goetzler, M. Guernsey, J. Young, J. Fujrman, and A. Abdelaziz, "The future of air conditioning for buildings," Navigant Consulting, Burlington, MA (2016).
3. B. Laillonne, "The future of air-conditioning," Enerdata, Grenoble (2019).
4. U.S. Energy Information Administration, "Residential electricity consumption by end use," 2015 Residential Energy Consumption Survey, Washington, DC (2015).
5. M. Santamouris and D. Kolokotsa, "Passive cooling dissipation techniques for buildings and other structures: The state of the art," Energy and Buildings **57**, 74–94 (2013).
6. K. Seyboth, L. Beurskens, O. Langniss, and R. E. Sims, "Recognising the potential for renewable energy heating and cooling," Energy Policy **36**(7), 2460–2463 (2008).
7. R. Fensholt, S. Horion, T. Tagesson, A. Ehammer, K. Grogan, F. Tian, S. Huber, J. Verbesselt, S. D. Prince, C. J. Tucker, and K. Rasmussen, "Assessment of vegetation trends in drylands from time series of earth observation data," in *Remote Sensing Time Series* (Springer, 2015), pp. 159–182.
8. Y. Zhai, Y. Ma, S. N. David, D. Zhao, R. Lou, G. Tan, R. Yang, and X. Yin, "Scalable-manufactured randomized glass-polymer hybrid metamaterial for daytime radiative cooling," Science **355**(6329), 1062–1066 (2017).
9. J. L. Kou, Z. Jurado, Z. Chen, S. Fan, and A. J. Minnich, "Daytime radiative cooling using near-black infrared emitters," ACS Photonics **4**(3), 626–630 (2017).
10. A. P. Raman, M. A. Anoma, L. Zhu, E. Rephaeli, and S. Fan, "Passive radiative cooling below ambient air temperature under direct sunlight," Nature **515**(7528), 540–544 (2014).
11. E. Rephaeli, A. Raman, and S. Fan, "Ultrabroadband photonic structures to achieve high-performance daytime radiative cooling," Nano Lett. **13**(4), 1457–1461 (2013).

Optics EXPRESS

12. Z. Chen, L. Zhu, A. Raman, and S. Fan, "Radiative cooling to deep sub-freezing temperatures through a 24-h day–night cycle," Nat. Commun. **7**(1), 13729 (2016).
13. M. M. Hossain, B. Jia, and M. Gu, "A metamaterial emitter for highly efficient radiative cooling," Adv. Opt. Mater. **3**(8), 1047–1051 (2015).
14. L. Zhu, A. Raman, and S. Fan, "Color-preserving daytime radiative cooling," Appl. Phys. Lett. **103**(22), 223902 (2013).
15. Z. Huang and R. Xiulin, "Nanoparticle embedded double-layer coating for daytime radiative cooling," Int. J. Heat Mass Transfer **104**, 890–896 (2017).
16. L. Zhu, A. Raman, K. X. Wang, and M. A. Anoma, "Radiative cooling of solar cells," Optica **1**(1), 32–38 (2014).
17. X. Ao, M. Hu, B. Zhao, N. Chen, G. Pei, and C. Zou, "Preliminary experimental study of a specular and a diffuse surface for daytime radiative cooling," Sol. Energy Mater. Sol. Cells **191**, 290–296 (2019).
18. H. Bao, C. Yan, B. Wang, X. Fang, C. Y. Zhao, and X. Ruan, "Double-layer nanoparticle-based coatings for efficient terrestrial radiative cooling," Sol. Energy Mater. Sol. Cells **168**, 78–84 (2017).
19. A. R. Gentle and G. B. Smith, "Radiative heat pumping from the earth using surface phonon resonant nanoparticles," Nano Lett. **10**(2), 373–379 (2010).
20. H. Y. Chan, S. B. Riffat, and J. Zhu, "Review of passive solar heating and cooling technologies," Renewable Sustainable Energy Rev. **14**(2), 781–789 (2010).
21. M. A. Kamal, "An overview of passive cooling techniques in buildings: design concepts and architectural interventions," Acta Technica Napocensis: Civil Engineering & Architecture **55**(1), 84–97 (2012).
22. U. Kortshagen, "Nonthermal plasma synthesis of semiconductor nanocrystals," J. Phys. D: Appl. Phys. **42**(11), 113001 (2009).
23. L. Mangolini, E. Thimsen, and U. Kortshagen, "High-yield plasma synthesis of luminescent silicon nanocrystals," Nano Lett. **5**(4), 655–659 (2005).
24. J. Kendrick and A. D. Burnett, "PDielec: The calculation of infrared and terahertz absorption for powdered crystals," J. Comput. Chem. **37**(16), 1491–1504 (2016).
25. V. A. Markel, "Introduction to the Maxwell Garnett approximation: tutorial," J. Opt. Soc. Am. A **33**(7), 1244–1256 (2016).
26. T. C. Choy, *Effective medium theory: principles and applications* (Oxford University Press, 2015).
27. J. Q. Xi, M. F. Schubert, J. K. Kim, E. F. Schubert, M. Chen, S. Y. Lin, W. Liu, and J. A. Smart, "Optical thin-film materials with low refractive index for broadband elimination of Fresnel reflection," Nat. Photonics **1**(3), 176–179 (2007).
28. S. I. Zaitsu, T. Jitsuno, M. Nakatsuka, T. Yamanaka, and S. Motokoshi, "Optical thin films consisting of nanoscale laminated layers," Appl. Phys. Lett. **80**(14), 2442–2444 (2002).
29. P. Yeh, A. Yariv, and C. S. Hong, "Electromagnetic propagation in periodic stratified media. I. General theory," J. Opt. Soc. Am. **67**(4), 423–438 (1977).
30. S. Molesky, C. J. Dewalt, and Z. Jacob, "High temperature epsilon-near-zero and epsilon-near-pole metamaterial emitters for thermophotovoltaics," Opt. Express **21**(S1), A96–A110 (2013).
31. M. M. Hossain and M. Gu, "Radiative cooling: Principles, progress, and potentials," Adv. Sci. **3**(7), 1500360 (2016).
32. G. F. Goya, "Handling the particle size and distribution of Fe3O4 nanoparticles through ball milling," Solid State Commun. **130**(12), 783–787 (2004).
33. S. Jeon and J. Shin, "Ideal spectral emissivity for radiative cooling of earthbound objects," Sci. Rep. **10**(1), 1–7 (2020).
34. . "U.S. Standard Atmosphere," U.S. Government Printing Office, Washington, D.C. (1976).
35. C. G. Granqvist and A. Hjortsberg, "Radiative cooling to low temperatures: General considerations and application to selectively emitting SiO films," J. Appl. Phys. **52**(6), 4205–4220 (1981).
36. J. C. Wright, "Accuracy of lowtran 7 and modtran in the 2.0-5.5-μm region," Appl. Opt. **33**(9), 1755–1759 (1994).
37. J. Wright, "Evaluation of LOWTRAN and MODTRAN for use over high zenith angle/long path length viewing," thesis (Rochester Institute of Technology, 1991).
38. L. W. Abreu and G. P. Anderson, "The MODTRAN 2/3 report and LOWTRAN 7 MODEL," Air Force Geophysics Lab, Hanscom AFB, MA (1996).
39. P. J. Launer, "Infrared analysis of organosilicon compounds: spectra-structure correlations," Silicone Compounds Register and Review 100 (1987).
40. A. L. Smith, "Infrared spectra-structure correlations for organosilicon compounds," Spectrochim. Acta **16**(1-2), 87–105 (1960).
41. A. L. Smith, *Analysis of Silicones* (Wiley-Interscience, 1974).
42. L. J. Bellamy, *The Infra-red Spectra of Complex Molecules*, 3rd ed. (Chapman and Hall, 1975).
43. A. H. Shivola, "Self-consistency aspects of dielectric mixing theories," IEEE Trans. Geosci. Remote Sensing **27**(4), 403–415 (1989).
44. I. H. Malitson, "Interspecimen comparison of the refractive index of fused silica," J. Opt. Soc. Am. **55**(10), 1205–1209 (1965).
45. C. Z. Tan, "Determination of refractive index of silica glass for infrared wavelengths by IR spectroscopy," J. Non-Cryst. Solids **223**(1-2), 158–163 (1998).
46. C. F. Bohren and D. R. Huffman, *Absorption and scattering of light by small particles* (John Wiley & Sons, 2008).

Optics EXPRESS

47. P. Chýlek, V. Srivastava, R. G. Pinnick, and R. T. Wang, "Scattering of electromagnetic waves by composite spherical particles: experiment and effective medium approximations," Appl. Opt. **27**(12), 2396–2404 (1988).
48. D. G. Stroud, "The effective medium approximations: Some recent developments," Superlattices Microstruct. **23**(3-4), 567–573 (1998).
49. K. K. Karkkainen, A. H. Sihvola, and K. I. Nikoskinen, "Effective permittivity of mixtures: numerical validation by the FDTD method," IEEE Trans. Geosci. Remote Sensing **38**(3), 1303–1308 (2000).
50. N. V. Voshchinnikov, G. Videen, and T. Henning, "Effective medium theories for irregular fluffy structures: aggregation of small particles," Appl. Opt. **46**(19), 4065–4072 (2007).
51. J. B. Bossa, K. Isokoski, D. M. Paardekooper, M. Bonnin, E. P. van der Linden, T. Triemstra, S. Cazaux, A. G. G. M. Tielens, and H. Linnartz, "Porosity measurements of interstellar ice mixtures using optical laser interference and extended effective medium approximations," Astron. Astrophys. **561**, A136 (2014).
52. T. Hulser, S. M. Schnurre, H. Wiggers, and C. Schulz, "Gas-phase synthesis of nanoscale silicon as an economical route towards sustainable energy technology," KONA Powder Part. J. **29**(0), 191–207 (2011).
53. N. Rao, S. Girshick, J. Heberlein, P. McMurry, S. Jones, D. Hansen, and B. Micheel, "Nanoparticle formation using a plasma expansion process," Plasma Chem. Plasma Process. **15**(4), 581–606 (1995).
54. M. Shigeta and A. B. Murphy, "Thermal plasmas for nanofabrication," J. Phys. D: Appl. Phys. **44**(17), 174025 (2011).
55. R. Gresback and Z. K. U. Holman, "Nonthermal plasma synthesis of size-controlled, monodisperse, freestanding germanium nanocrystals," Appl. Phys. Lett. **91**(9), 093119 (2007).
56. A. Donev, I. Cisse, D. Sachs, E. A. Variano, F. H. Stillinger, R. Connelly, S. Torquato, and P. M. Chaikin, "Improving the density of jammed disordered packings using ellipsoids," Science **303**(5660), 990–993 (2004).
57. F. A. Dullien, *Porous media: fluid transport and pore structure* (Academic Press, 2012).
58. J. F. Varner, N. Eldabagh, D. Volta, R. Eldabagh, and J. J. Foley IV, "WPTherml: A Python Package for the Design of Materials for Harnessing Heat," Journal of Open Research Software **7**(28), 1 (2019).
59. S. J. Byrnes, "Multilayer optical calculations," arXiv preprint arXiv:1603.02720 (2016).
60. F. X. Kneizys, E. P. Shettle, L. W. Abreu, J. H. Chetwynd, and G. P. Anderson, "Users guide to LOWTRAN 7. No. AFGL-TR-88-0177," Air Force Geophysics Lab, Hanscom AFB, MA (1988).